

Supporting Information

Three-dimensional conductive copper-organic framework with dual-redox center for high-performance aqueous zinc battery

Jiacun wang^{ab}, Yuanxiang Gu^{b*} and Qingliang Lv^{a*}

^a Key Laboratory of Eco-chemical Engineering, International Science and Technology Cooperation Base of Eco-chemical Engineering and Green Manufacturing, College of Chemical Engineering, Qingdao University of Science and Technology, Qingdao 266042, PR China

^b College of Environment and Safety Engineering, Qingdao University of Science and Technology, Qingdao 266042, PR China

Corresponding authors: qinglianglv@qust.edu.cn; gyx0524@126.com.

Chemicals

2,3,5,6-Tetraaminobenzoquinone (TABQ) was purchased from the Jilin Chinese Academy of Science-Yanshen Technology Co. Ltd, $\text{Cu}(\text{NO}_3)_2 \cdot 3\text{H}_2\text{O}$ (AR) was purchased from the Sinopharm Chemical Reagent Co., Ltd. All chemicals and materials were used without further purification.

Synthesis of Cu-TAPT

50.4 mg of TABQ was suspended in 12 ml of distilled water. Then 108.7 mg of $\text{Cu}(\text{NO}_3)_2 \cdot 3\text{H}_2\text{O}$ in 6 ml of distilled water was added to the suspension. The mixture was heated to 120 °C in a round-bottom flask for three days and allowed to cool to room temperature. Black powder was obtained by vacuum filtration and washed with water several times.

Physicochemical Characterization

The crystallographic structure of Cu-TAPT was identified by an X-ray diffraction instrument (Bruker D8 Advance, Germany Cu $K\alpha$ radiation). EDX chemical mapping, lattice spacing, and morphological size of Cu-TAPT were analyzed by the Field emission transmission electron microscope (FETEM JEF-F200, JAPAN). The element state was detected via X-ray photoelectron spectroscopy (XPS Escalab 250X Thermo Fisher Scientific). The Fourier-transformed infrared (FT-IR) spectra were collected on professional equipment (Nicolet iS50 ThermoFisher American).

Thermal stability was evaluated in the air atmosphere by thermogravimetric analysis (TGA NETZSCH STA 449 F5 Germany). The BET surface area and pore size distributions were measured on an accelerated surface area and porosimetry analyzer (ASAP2020 Micromeritics).

Electrochemical Measurements

The electrochemical measurements of Cu-TAPT were conducted in CR2032 coin cells with Zn metal anode with 2.5 M L⁻¹ Zinc trifluoromethanesulfonate Zn (OTf)₂. The Cu-TAPT electrode is prepared by mixing 50 wt% of Cu-TAPT powder, 40 wt% of carbon black, and 10 wt % of Polytetrafluoroethylene (PTFE), and then uniformly pressing it into a thin film. Finally, after being dried at 60 °C for 12 hours in a vacuum oven, the thin film is cut into square sheets and put on the Titanium (Ti) collector (diameter of 12 mm and thickness of 200 μm).

Galvanostatic charge and discharge profiles, rate charge and discharge profiles and Galvanostatic Intermittent Titration Technique (GITT) data were collected by using a LAND-CT3002A battery-testing instrument (LAND Electronic Co., Wuhan China). Cyclic Voltammetry (CV) measurements and Electrochemical Impedance Spectroscopy (EIS, frequency range from 0.01Hz-1M Hz) were performed on a (ZAHNHER biologic, France) electrochemical workstation.

Theoretical specific capacity calculation is based on the following equation:

$$C = \frac{26.8n}{M} \text{ (Ah g}^{-1}\text{)}$$

Where n is the electron-transfer number; M refers to the molar weight of the Cu-TAPT structural unit; 26.8 (Ah g⁻¹) is the amount of electricity released by 1 mole of active substance participating in a chemical reaction. Thus, for Cu-TAPT MOF, the molar weight is 488 g mol⁻¹, so the theoretical capacity is 274.6 mAh g⁻¹.

As for the GITT, the Zn²⁺ diffusion coefficients were calculated according to the following formula:

$$D = \frac{4L^2\Delta E_s}{\pi\tau \Delta E_t}$$

Where L refers to the ion diffusion length (cm, the distance between anode and cathode materials) ΔE_s and ΔE_t are the steady-state potential change (V) caused by the current pulse and the direct change of voltage (V) before relaxation, respectively. τ is the setting time (30 min)

I-V curves of Cu-TAPT

The electrical conductivity (σ) is calculated according to the equation:

$$\sigma = \frac{L}{R \pi \left(\frac{D}{2}\right)^2}$$

Where L is the thickness and D is the diameter of Cu-TAPT pellet respectively. π is the fundamental constant with the value of 3.14. R refers to the electric resistance, namely, the reciprocal of slope of I-V curve. Here, R=294 Ω , L=0.87 mm, and D=12.87 mm.

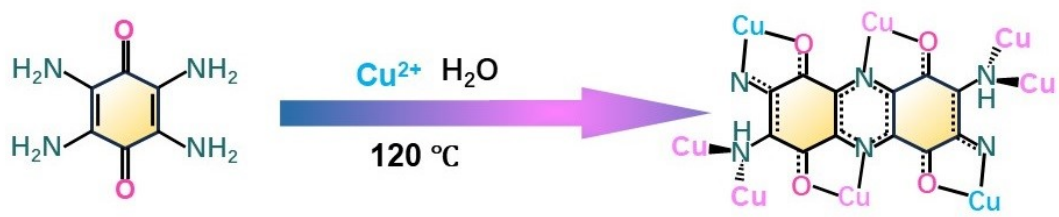


Fig. S1 Synthesis route of Cu-TAPT.

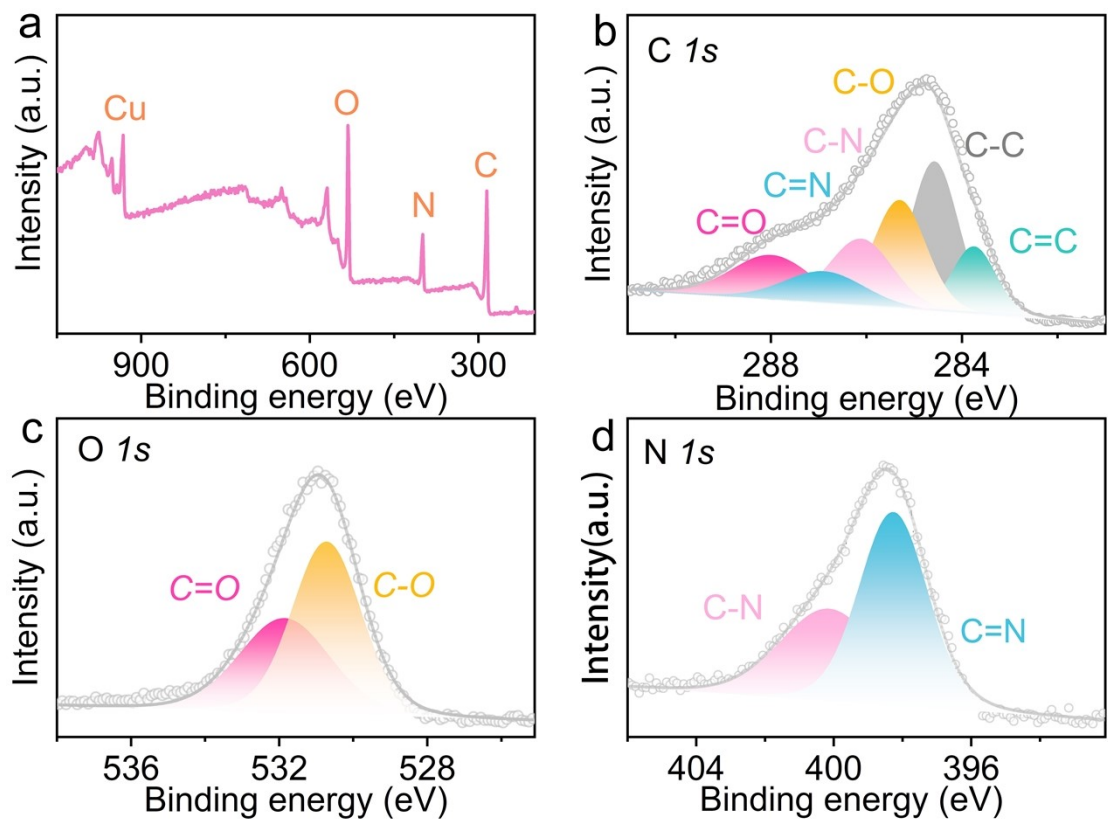


Fig. S 2 (a). XPS survey spectrum of Cu-TAPT, (b-d). XPS spectrum of C1s, N1s, O1s.

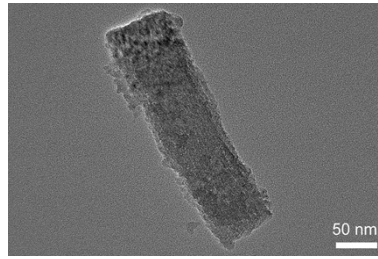


Fig. S3. TEM image of the Cu-TAPT.

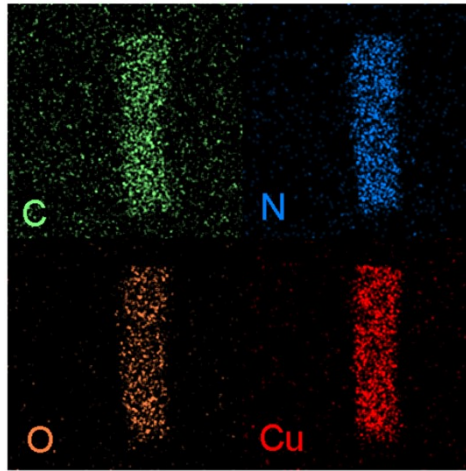


Fig. S4 EDS mappings of Cu-TAPT.

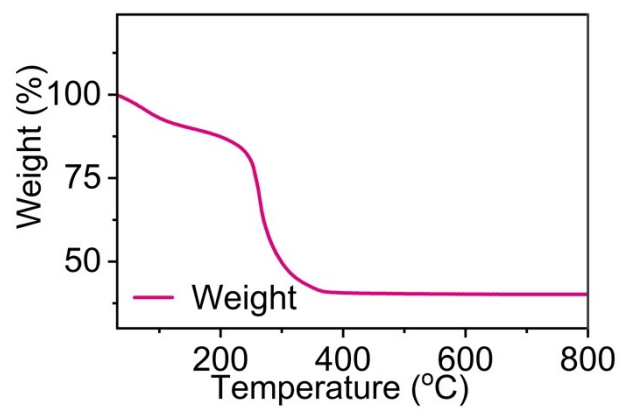


Fig. S5 TGA curves of Cu-TAPT in air atmosphere at a heating rate of 10 °C min⁻¹.

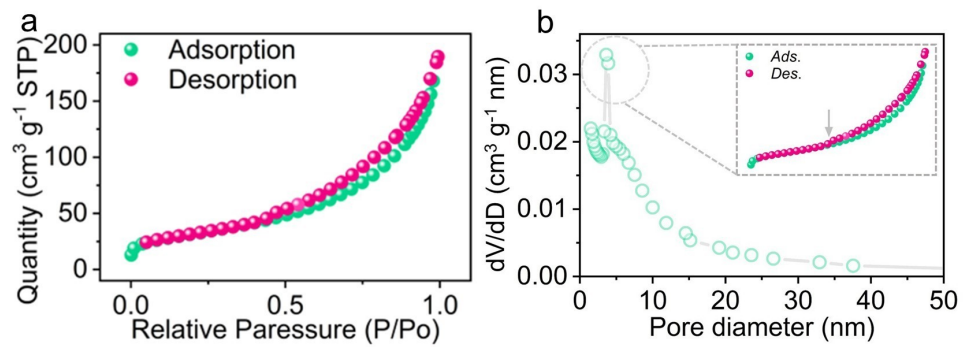


Fig S6 (a) N_2 adsorption-desorption isotherm of the Cu-TAPT. (b) Pore size distribution analysis of Cu-TAPT.

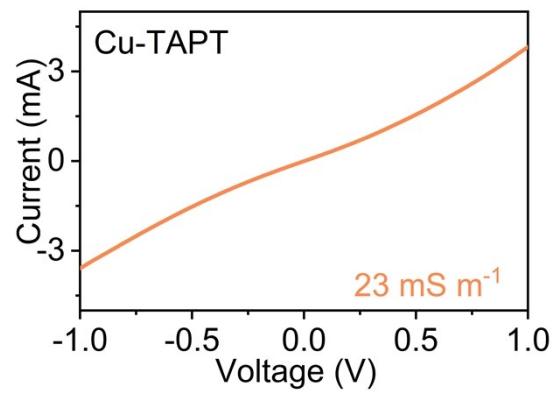


Fig. S7 The I - V curve of Cu-TAPT.

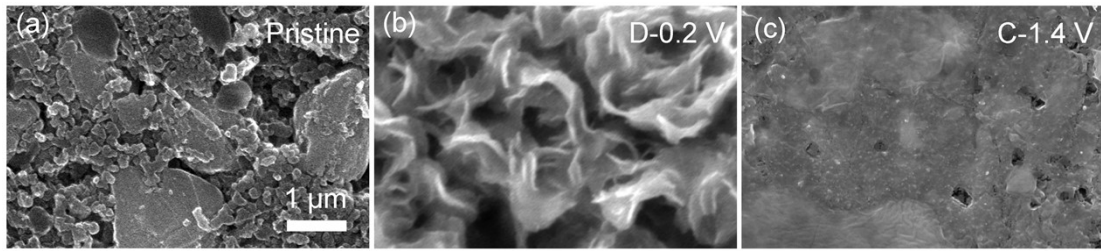


Fig. S8 The SEM image of the Cu-TAPT electrode surface during the battery operation.

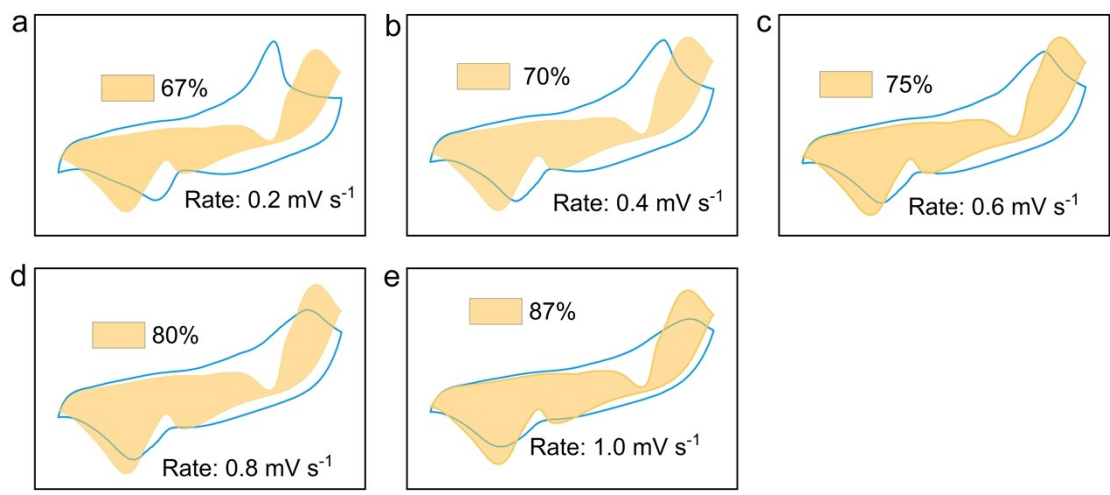


Fig. S9 Contribution rate of pseudocapacitance at different scanning speeds.

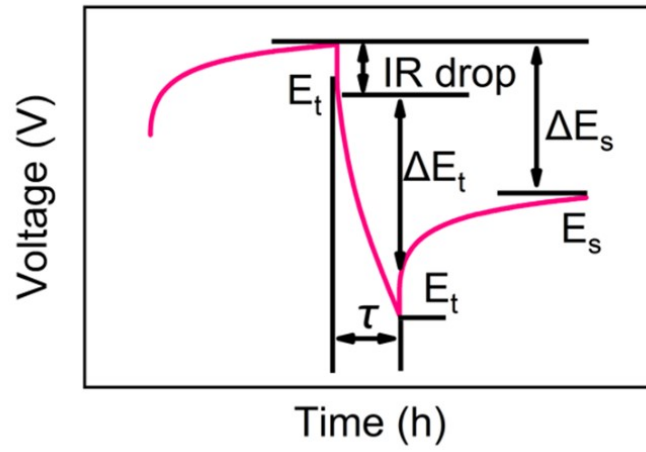


Fig S10 Schematic illustration of selected steps from the GITT curve during the discharging process.

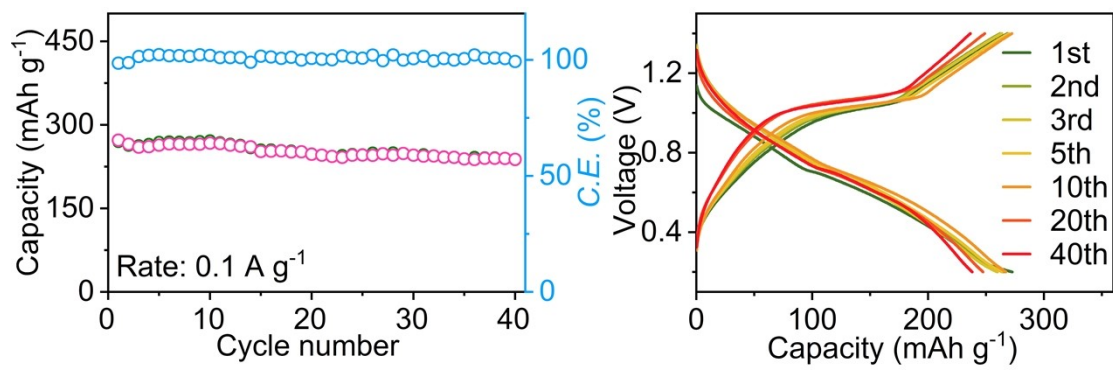


Fig. S11 Discharge/charge curves of Cu-TAPT at the current density of 0.1 A g⁻¹.

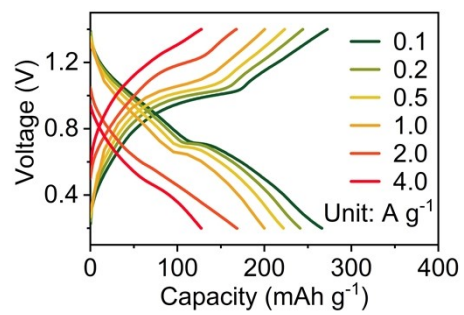


Fig. S12 Discharge/charge rate curves of Cu-TAPT.

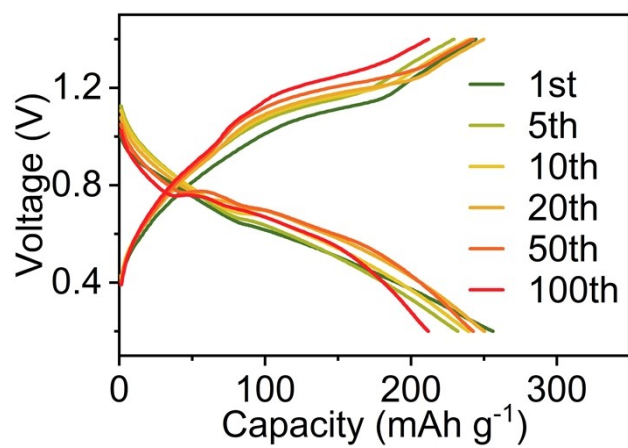


Fig. S13 Discharge/charge curves of Cu-TAPT at the current density of 0.5 A g⁻¹.

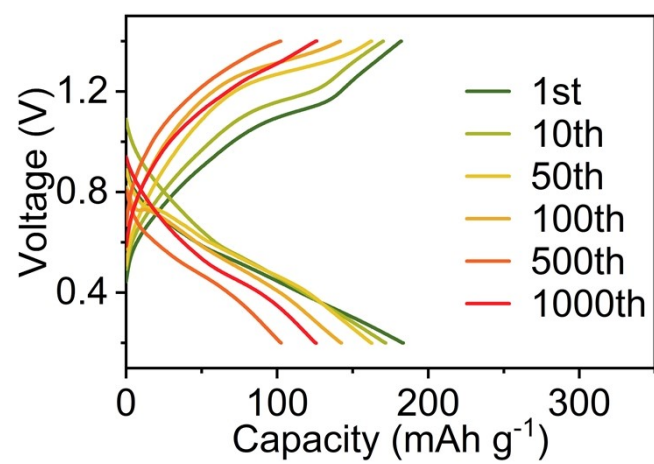


Fig. S14 Discharge/charge curves of Cu-TAPT at the current density of 4 A g⁻¹.

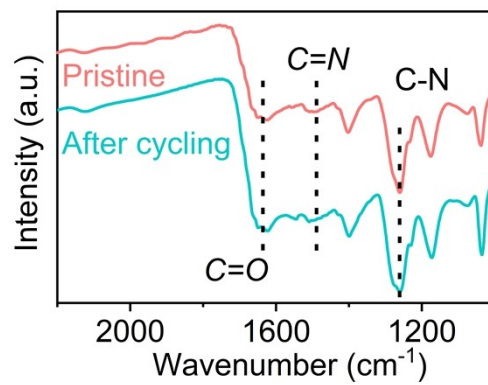


Fig. S15 FTIR spectra of pristine and cycling Cu-TAPT electrodes.

Table S1 Atomic coordinates of Cu-TAPT.

Atom	x	y	z	Occ.
Cu1	1	0.5	0.5	1
Cu2	0.3468	0.6897	0.5	1
C1	0.7461	0.5124	0.5	1
C2	0.7981	0.6049	0.5	1
C3	0.7203	0.6798	0.5	1
C4	0.5964	0.6698	0.5	1
C5	0.5477	0.5813	0.5	1
C6	0.619	0.5079	0.5	1
N1	0.9135	0.6064	0.5	1
N2	0.7607	0.7637	0.5	1
N3	0.4282	0.5741	0.5	1
O1	0.8071	0.4481	0.5	1
O2	0.5298	0.7352	0.5	1

Orthorhombic, space group *Pnmm*, a = 11.41 Å, b = 15.16 Å, c = 3.12 Å $\alpha = \beta = \gamma = 90^\circ$,

V=539.68 Å³.

Table S2 Comparison of the electrochemical performance with other previously reported MOFs electrodes.

Cathode materials	Electrolyte	Capacity (mAh g ⁻¹)	Current density (A g ⁻¹)	Reference
Mn-H3BTC	2 M Zn(CF ₃ SO ₃) ₂	98	3	[1]
PA-COF	1M ZnSO ₄	94	1	[2]
Mn-BDC	2 M ZnSO ₄ +0.1 M MnSO ₄	137	0.3	[3]
Cu-HHTP	3 M Zn(CF ₃ SO ₃) ₂	93	4	[4]
Mn-BTC	2 M ZnSO ₄ +0.1 M MnSO ₄	46	1	[5]
Cu-TCNQ	2 M Zn(CF ₃ SO ₃) ₂	61	2	[6]
HA-COF	2.0 M ZnSO ₄	61	5	[7]
Ni-Ndi-trz	2 M ZnSO ₄	90.7	3	[8]
PTCDI	2M ZnSO ₄	123	3	[9]
KNF-086	0.5 M Zn(ClO ₄) ₂	26.8	0.056	[10]
PoPD	2 M ZnSO ₄	95	5	[11]
P3Q-t	2 M ZnSO ₄	100	3	[12]
PPPA	2 M Zn(CF ₃ SO ₃) ₂	92	5	[13]
BBPD	2 M ZnSO ₄	88	2	[14]
APh-NQ@CNT	2 M ZnSO ₄	139	0.1	[15]
DTT	2 M ZnSO ₄	79	2	[16]
NTCDI	2 M ZnSO ₄	152	1	[17]
NTCDA	2 M ZnSO ₄	25	2	[18]
π-PMC	2 M ZnCl ₂	102.7	0.2	[19]
PQTU	1 M ZnSO ₄	111	0.1	[20]
2Cl-NQ	2 M ZnSO ₄	91	5	[21]
PTZAN	Zn(CF ₃ SO ₃) ₂ (TMP:EC:DEC=1:1:1)	110	1	[22]
PTD-1	2 M ZnSO ₄	100	1	[23]
PASP-TEMPO	1M ZnClO ₄	120	2.4	[24]
<i>Cu-TAPT</i>	<i>2.5Zn(CF₃SO₃)₂</i>	<i>126</i>	<i>4</i>	<i>This work</i>

Reference:

- [1] C. Yin, C. Pan, X. Liao, Y. Pan, L. Yuan, *ACS Appl. Mater. Interfaces*, 2021, **13**, 35837-35847.
- [2] W. Wang, V. S. Kale, Z. Cao, S. Kandambeth, W. Zhang, J. Ming, P. T. Parvatkar, E. Abou-Hamad, O. Shekhah, L. Cavallo, M. Eddaoudi, H. N. Alshareef, *ACS Energy Lett.*, 2020, **5**, 2256-2264.
- [3] W. Gou, H. Chen, Z. Xu, Y. Sun, X. Han, M. Liu, Y. Zhang, *Energy Adv.*, 2022, **1**, 1065-1070.
- [4] K. W. Nam, S. S. Park, R. Dos Reis, V. P. Dravid, H. Kim, C.A. Mirkin, J. F. Stoddart, *Nat. Commun.*, 2019, **10**, 4948.
- [5] X. Pu, B. Jiang, X. Wang, W. Liu, L. Dong, F. Kang, C. Xu, *Nano-Micro Lett.*, 2020, **12**, 152.
- [6] L. Zhang, Y. Chen, Z. Jiang, J. Chen, C. Wei, W. Wu, S. Li, Q. Xu, *Energy Environ. Mater.*, 2022, **7**, e12507.
- [7] W. Wang, V. S. Kale, Z. Cao, Y. Lei, S. Kandambeth, G. Zou, Y. Zhu, E. Abouhamad, O. Shekhah, L. Cavallo, M. Eddaoudi, H. N. Alshareef, *Adv. Mater.*, 2021, **33**, 2103617.
- [8] Y. Liu, Z. Li, Y. Han, Z. Ji, H. Li, Y. Liu, Y. Wei, C. Chen, X. He, M. Wu, *ChemSusChem.*, 2023, **16**, e202202305.
- [9] N. Liu, X. Wu, Y. Zhang, Y. Yin, C. Sun, Y. Mao, L. Fan, N. Zhang, *Adv. Sci.*, 2020, **7**, 2000146.
- [10] M. S. Chae, J. W. Heo, H. H. Kwak, H. Lee, S. T. Hong, *J. Power Sources*, 2017, **337**, 204e211.
- [11] S. Zhang, S. Long, H. Li, Q. Xu, *Chem. Eng. J.*, 2020, **400**, 125898.
- [12] X. Wang, J. Tang, W. Tang, *Adv. Funct. Mater.*, 2022, **32**, 2200517.
- [13] F. Ye, Q. Liu, H. Dong, K. Guan, Z. Chen, N. Ju, L. Hu, *Angew. Chem. Int. Ed.*, 2022, **134**, e202214244.
- [14] Q. Wang, Y. Liu, C. Wang, X. Xu, W. Zhao, Y. Li, H. Dong, *Chem. Eng. J.*, 2023, **451**, 138776.
- [15] 23 J. Kumankuma-Sarpong, S. Tang, W. Guo, Y. Fu, *ACS Appl. Mater.*, 2021, **13**, 4084-4092.
- [16] 24 Y. Wang, C. Wang, Z. Ni, Y. Gu, B. Wang, Z. Guo, Z. Wang, D. Bin, J. Ma, Y. Wang, *Adv. Mater.*, 2020, **32**, 2000338.

- [17] X. Wang, L. Chen, F. Lu, J. Liu, X. Chen, G. Shao, *ChemElectroChem.*, 2019, **6**, 3644-3647.
- [18] M. Ghosh, V. Vijayakumar, M. Kurian, S. Dilwale, S. Kurungot, *Dalton Trans.*, 2021, **50**, 4237-4243.
- [19] D. Xu, H. Zhang, L. Zhou, X. Gao, X. Lu, *ChemPhysMater.*, 2022, **1**, 86-101.
- [20] C. Guo, Y. Liu, L. Wang, D. Kong, J. Wang, *ACS SUSTAIN CHEM ENG.*, 2022, **10**, 213-223.
- [21] J. Wu, W. Xu, Y. Lin, X. Shi, F. Yang, X. Lu, *J. Power Sources*, 2021, **483**, 229114.
- [22] X. Qiu, J. Xu, K. Zhou, X. Huang, M. Liao, Y. Cao, G. Zhou, P. Wei, Y. Wang, *Angew. Chem. Int. Ed.*, 2023, **60**, e202304036.
- [23] N. Wang, Z. Guo, Z. Ni, J. Xu, X. Qiu, J. Ma, P. Wei, Y. Wang, *Angew. Chem. Int. Ed.*, 2021, **60**, 20826-20832.
- [24] Y. Deng, C. Teng, Y. Wu, K. Zhang, L. Yan, *Chemsuschem*, 2022, **15**, e202102710.